

## **Screening of polymer type and weathering in macro and mesoplastics found in lake and river beaches using a combined chemometric approach**

Nicolas Nayrac <sup>1</sup>, Jean-Philippe Bellenger <sup>1</sup>, Pedro A. Segura <sup>1,\*</sup>

\* Tel: 1-(819) 821-7922. Fax: 1-(819) 821-8019. E-mail: pa.segura@usherbrooke.ca

<sup>1</sup> Department of Chemistry, Université de Sherbrooke, Sherbrooke, QC J1K 2R1

### **Supplementary Information**

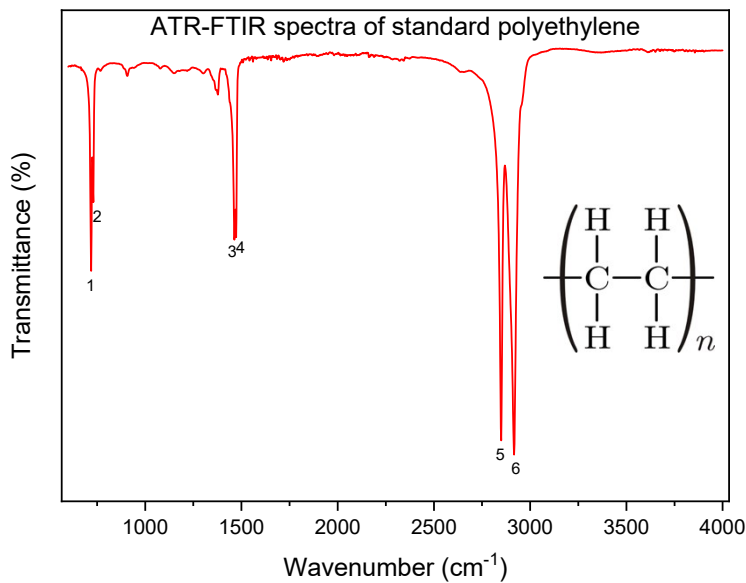


**Figure S1.** FTIR spectrum of a standard polyethylene sample.

**Table S1.** Main infrared vibration modes corresponding to a polyethylene standard sample.

Peak number	Wavenumber ( $\text{cm}^{-1}$ )	Vibration mode & functional group
<b>1</b>	719.4	Amorphous Rock Methylene (-CH <sub>2</sub> )
<b>2</b>	730.6	Crystalline Rock Methylene (-CH <sub>2</sub> )
<b>3</b>	1436.0	Amorphous Bending Methylene (-CH <sub>2</sub> )
<b>4</b>	1472.3	Crystalline Bending Methylene (-CH <sub>2</sub> )
<b>5</b>	2849.5	Stretching Methylene (-CH <sub>2</sub> )
<b>6</b>	2916.6	Stretching Methylene (-CH <sub>2</sub> )

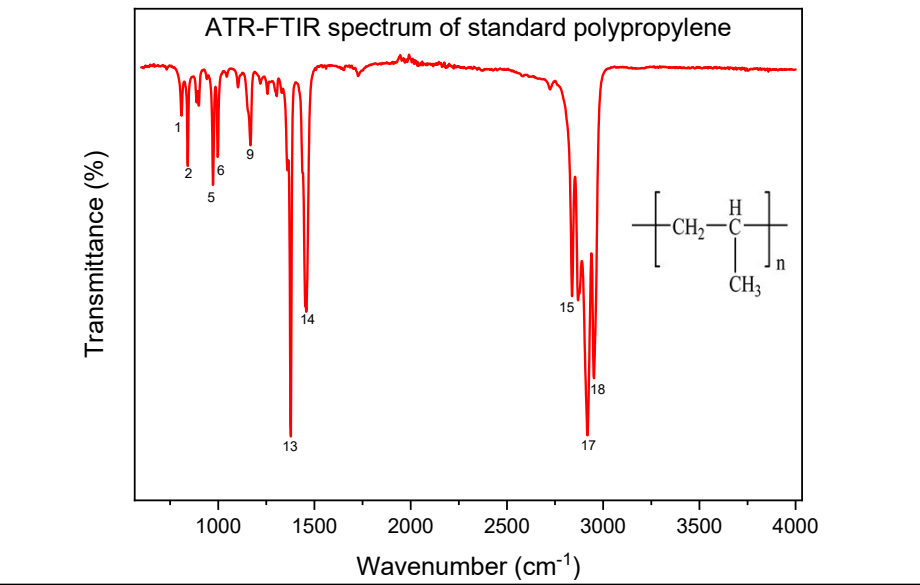


**Figure S2.** FTIR spectrum of a standard polypropylene sample.

**Table S2.** Main infrared vibration modes corresponding to a polypropylene standard sample ( $\rho$  : rocking,  $v$  : stretching,  $\tau$  : twisting,  $\delta$  : bending,  $\omega$  : wagging ).

Peak number	Wavenumber ( $\text{cm}^{-1}$ )	Vibration mode & functional group
<b>1</b>	808.8	
<b>2</b>	842.4	Rocking $\rho\text{CH}_2$
<b>3</b>	889.0	
<b>4</b>	898.3	
<b>5</b>	972.8	Rocking $\rho\text{CH}_3$
<b>6</b>	997.1	
<b>7</b>	1043.7	Stretching $v\text{C}-\text{CH}_3$
<b>8</b>	1103.3	
<b>9</b>	1158.6 ; 1166.7	Stretching $v\text{CC}_b$
<b>10</b>	1218.8	Twisting $\tau\text{CH}_2$
<b>11</b>	1256.1	Bending $\delta\text{CH}$
<b>12</b>	1304.6	Wagging $\omega\text{CH}_2$
<b>13</b>	1375.4 ; 1360.5	Symmetric Bending $\delta\text{CH}_3$
<b>14</b>	1453.7	Asymmetric Bending $\delta\text{CH}_3$
<b>15</b>	2840.2	Symmetric Stretching $v\text{CH}_2$
<b>16</b>	2870.0	Symmetric Stretching $v\text{CH}_3$
<b>17</b>	2918.5	Asymmetric Stretching $v\text{CH}_2$
<b>18</b>	2952.1	Asymmetric Stretching $v\text{CH}_3$

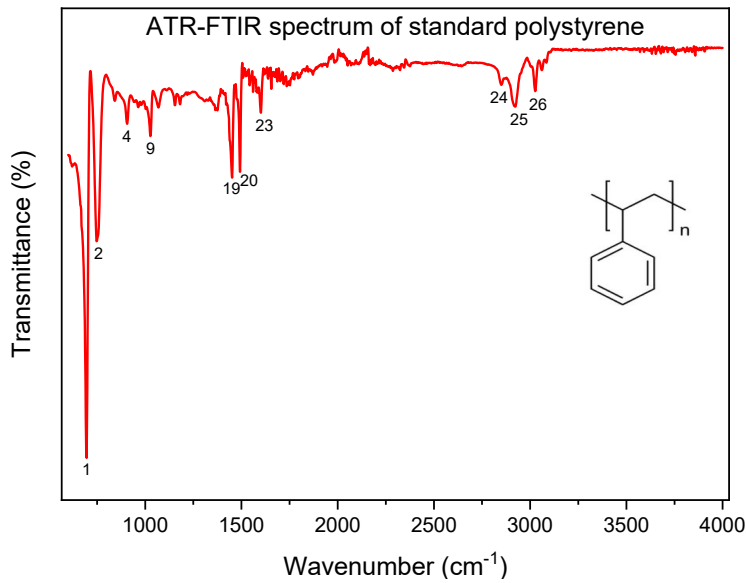


**Figure S3.** FTIR spectrum of a standard polystyrene sample.

**Table S3.** Main infrared vibration modes corresponding to a polystyrene standard sample ( $\rho$  : rocking,  $\nu$  : stretching,  $\tau$  : twisting,  $\delta$  : bending,  $\omega$  : wagging ).

Peak number	Wavenumber ( $\text{cm}^{-1}$ )	Vibration mode & functional group
1	695.1	$\nu_{11}(\text{B}_2)$
2	749.2	$\nu_{10\text{B}}(\text{B}_2)$
3	842.4	$\nu_{10\text{A}}(\text{A}_2)$
4	905.7	$\nu_{17\text{B}}(\text{B}_2)$
5	943.1	$\nu_4 + \nu_{16\text{A}} = 950$ ( $\text{B}_1$ )
6	963.5	$\nu_{17\text{A}}(\text{A}_2)$
7	980.3	$\nu_{10\text{B}} + \nu_{16\text{B}} = 978$ ( $\text{A}_1$ )
8	1002.7	$\nu_1(\text{A}_1)$
9	1026.9	$\nu_{18\text{A}}(\text{A}_1)$
10	1069.7	$\nu'_{18\text{B}}(\text{B}_1)$
11	1112.6	$\nu_{11} + \nu_{16\text{A}} = 1110$ ( $\text{B}_1$ )
12	1155.5	$\nu'_{15}(\text{B}_1)$
13	1181.6	$\nu(\text{CC})_{\text{helix}}$
14	1198.3	$\nu_{8\text{A}}(\text{A}_1)$
15	1310.2	$\nu_{14}(\text{B}_1), \tau(\text{CH}_2)$
16	1326.9	$\nu'_{3}(\text{B}_1)$
17	1364.2	$\delta(\text{CH})$
18	1375.4	
19	1451.8	$\nu_{19\text{B}}(\text{B}_1)$
20	1492.8	$\nu_{19\text{A}}(\text{A}_1)$
21	1541.3	$\nu_{11} + \nu_{10\text{A}} = 1542$ ( $\text{B}_1$ )
22	1584.1	$\nu_{9\text{A}}(\text{A}_1)$
23	1600.9	$\nu_{9\text{B}}(\text{B}_1)$
24	2851.4	$\nu_{\text{S}}(\text{CH}_2)$
25	2924.1	$\nu_{\text{a}}(\text{CH}_2)$
26	3026.6	$\nu'_{2}(\text{A}_1)$
27	3062.0	$\nu'_{20\text{A}}(\text{A}_1)$
28	3084.4	$\nu_{20\text{B}}(\text{B}_1)$

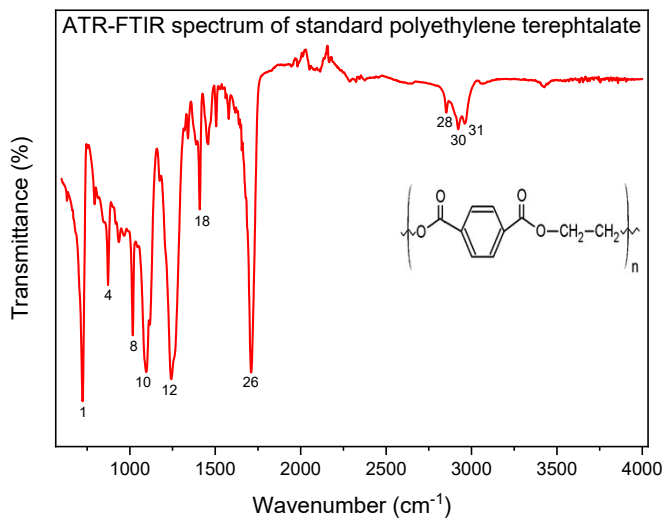


**Figure S4.** FTIR spectrum of a standard PET sample.

**Table S4.** Main infrared vibration modes corresponding to a PET sample ( $\rho$  : rocking,  $\nu$  : stretching,  $\tau$  : twisting,  $\delta$  : bending,  $\omega$  : wagging).

Peak number	Wavenumber ( $\text{cm}^{-1}$ )	Vibration mode & functional group
1	723.1	$\nu_{11}(\text{B}_{1u})$
2	793.9	$\rho(\text{C=O}) + \delta(\text{CCO})$
3	846.1	$\rho(\text{CH}_2)$
4	874.1	$\nu_{17B}(\text{B}_{1u})$
5	900.2	$\delta(\text{COC}) + \omega(\text{C=O})$
6	935.6	-
7	967.2	$\nu_{12}(\text{B}_{2u})$
8	1017.6	$\nu_{18A}(\text{B}_{2u})$
9	1045.5	$\nu(\text{C-C})$
10	1095.8	$\nu_{15}(\text{B}_{3u}), \nu(\text{O-C})$ (amorphous)
11	1116.3	$\nu(\text{O-C})$ (crystalline)
12	1176.0	$\nu_{9A}(\text{A}_1)$
13	1243.1	$\nu(\text{C-O})$
14	1261.7	
15	1340.0	$\nu_{13}(\text{B}_{2u})$
16	1371.7	$\nu_2'(\text{A}_1)$
17	1388.4	$\nu_5(\text{B}_{3g} : 978) + \nu_{16A}(\text{A}_u : 404) = 1382(\text{B}_{3u})$
18	1408.9	$\nu_5(\text{B}_{3g} : 978) + \nu_{16B}(\text{B}_{1u} : 430) = 1408(\text{B}_{2u})$
19	1438.8	-
20	1459.3	$\delta(\text{CH}_2)$
21	1472.3	$\nu_{19B}(\text{B}_{3u}), \delta(\text{CH}_2)$
22	1504.0	$\nu_{19A}(\text{B}_{2u})$
23	1559.9	$\nu(\text{O-C}) + \delta(\text{CCO})$
24	1580.4	$\nu_{8A}(\text{A}_1)$
25	1617.7	$\nu_{8B}(\text{B}_1)$
26	1712.7	$\nu(\text{C=O})$
27	1832.0	$\nu_{10A}(\text{B}_{2g} : 853) + \nu_{17A}(\text{A}_u : 977) = 1830(\text{B}_{2u})$
28	2853.3	-
29	2881.2	-
30	2922.2	$\nu_S(\text{CH}_2)$
31	2961.4	$\nu_a(\text{CH}_2)$
32	3058.3	$\nu_{20A}(\text{B}_{2u})$

33	3425.4	$2 \times v(C=O)$
----	--------	-------------------

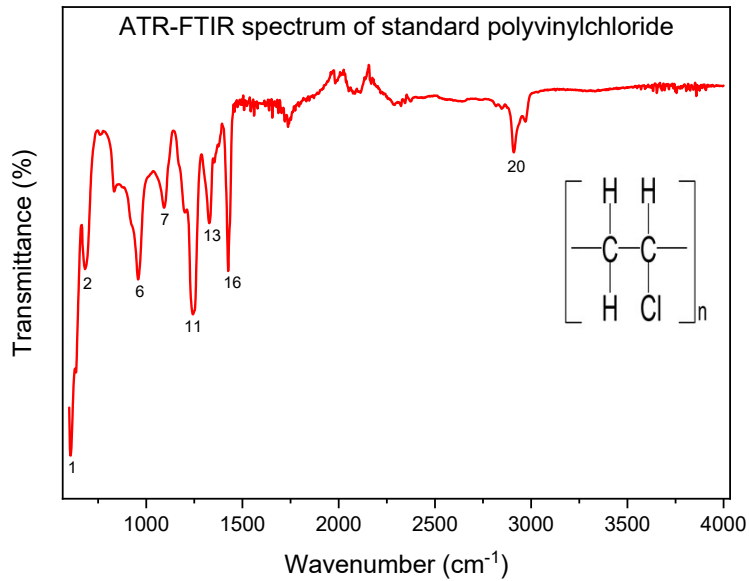


**Figure S5.** FTIR spectrum of a standard polyvinylchloride sample.

**Table S4.** Main infrared vibration modes corresponding to a polyvinylchloride standard sample ( $\rho$  : rocking,  $v$  : stretching,  $\tau$  : twisting,  $\delta$  : bending,  $\omega$  : wagging).

Pic n°	Nombre d'onde ( $\text{cm}^{-1}$ )	Mode de vibration & groupe fonctionnel
1	611.3	$v(\text{CCl})$ (Cl trans to H)
2	684.0	$v(\text{CCl})$ (Cl trans to C)
3	762.2	$v(\text{CCl})$ ( $B_{2u}$ ) + $v(\pi/2)$ ( $B_{1g}$ ) = 786 ( $B_{3u}$ )
4	833.1	$\rho(\text{CH}_2)_{0i}$ ( $B_{3u}$ )
5	922.5	$v_+(\pi/2)_0$ ( $B_{1u}$ )
6	957.9	$\rho(\text{CH}_2)_{i_i}$ ( $B_{1u}$ )
7	1094.0	$v_+(0)_0$ ( $B_{3u}$ )
8	1118.2	$v_+(\pi)_i$ ( $B_{3u}$ )
9	1170.4	$\tau(\text{CH}_2)_{00}$ ( $B_{2u}$ )
10	1200.2	$\rho(\text{CH}_2)_{0i}$ ( $B_{3u}$ ) + $\delta(\text{CCl})_{ii}$ ( $A_g$ ) ( $\approx 363$ ) = 1196 ( $B_{3u}$ )
11	1243.1	$2 \times 615 = 1230$
12	1252.4	$\delta(\text{CH})_{i0}$ ( $B_{2u}$ )
13	1328.8	$\delta(\text{CH})_{0i}$ ( $B_{1u}$ )
14	1353.0	$\delta(\text{CH})(\text{A}_g) + R'_0$ ( $B_{1u}$ ) = 1356 ( $B_{1u}$ )
15	1375.4	$\omega(\text{CH}_2)_{ii}$ ( $B_{3u}$ )
16	1425.7	$\delta(\text{CH}_2)_{i0}$ ( $B_{2u}$ )
17	1431.3	$\delta(\text{CH}_2)$
18	2817.9	$v(\text{CH})_{i0}$ ( $B_{2u}$ )
19	2845.8	$v_s(\text{CH}_2)_{i0}$ ( $B_{2u}$ )
20	2909.2	$v_a(\text{CH}_2)_{ii}$ ( $B_{1u}$ )
21	2939.0	$v_a(\text{CH}_2)_{0i}$ ( $B_{3u}$ )
22	2972.6	$v(\text{CH})_{0i}$ ( $B_{1u}$ )

Note: Despite the absence of a carbonyl group in the structure of PVC, a strong band at  $1731 \text{ cm}^{-1}$  was also detected in the FTIR spectra of PVC consumer product samples. The use of heat stabilizers containing carbonyl groups (e.g., metal carboxylates, maleates, mercaptides, oxirane) required to overcome the poor thermal stability of PVC may explain the presence of such band <sup>1</sup>. Likewise, the low flexibility of PVC is

often reduced by the addition of phthalate plasticizers such as butyl benzyl phthalate, diisononyl phthalate (DINP) and dicyclo-hexyl phthalate, dihexyl phthalate). For example, common flexible PVC products such as boots or gloves contain DINP at a concentration level of roughly 80 parts per hundred resin by weight (i.e., 80 g of DINP are added for every 100 g of PVC resin). Moreover, in children's toys, phthalates are also incorporated in a high proportion (10-40% w/w)<sup>2</sup>. Given the presence of two carbonyl groups in phthalates, it is not astonishing that C=O bonds are detected in PVC samples.

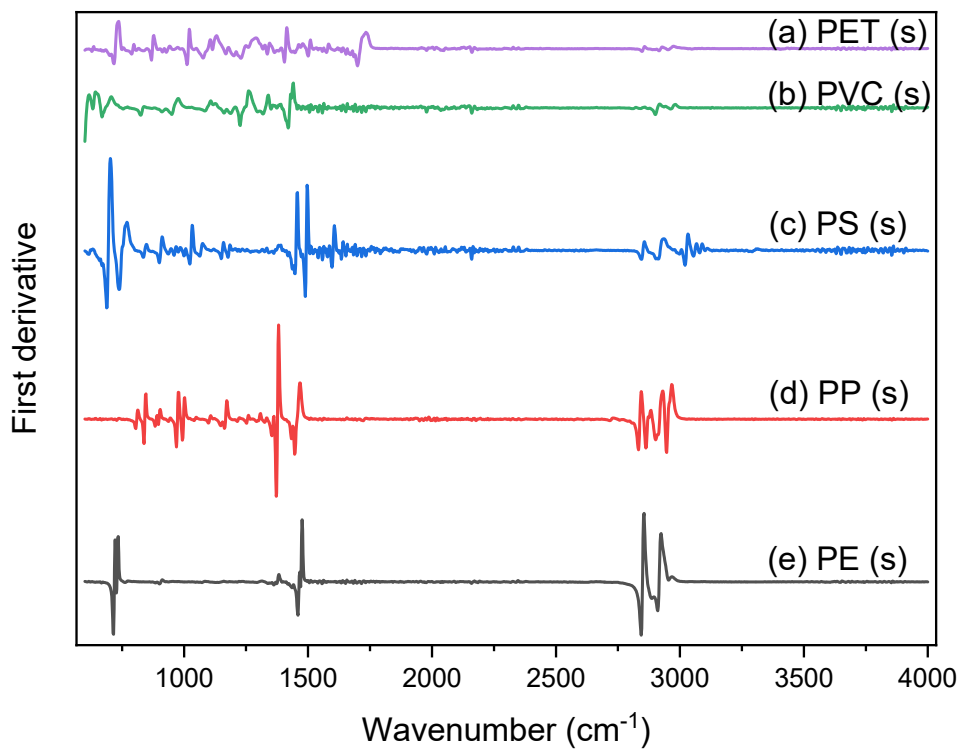


**Figure S6.** Preprocessed FTIR spectra of standard (a) polyethylene terephthalate, (b) polyvinylchloride, (c) polystyrene, (d) polypropylene and (e) polyethylene.

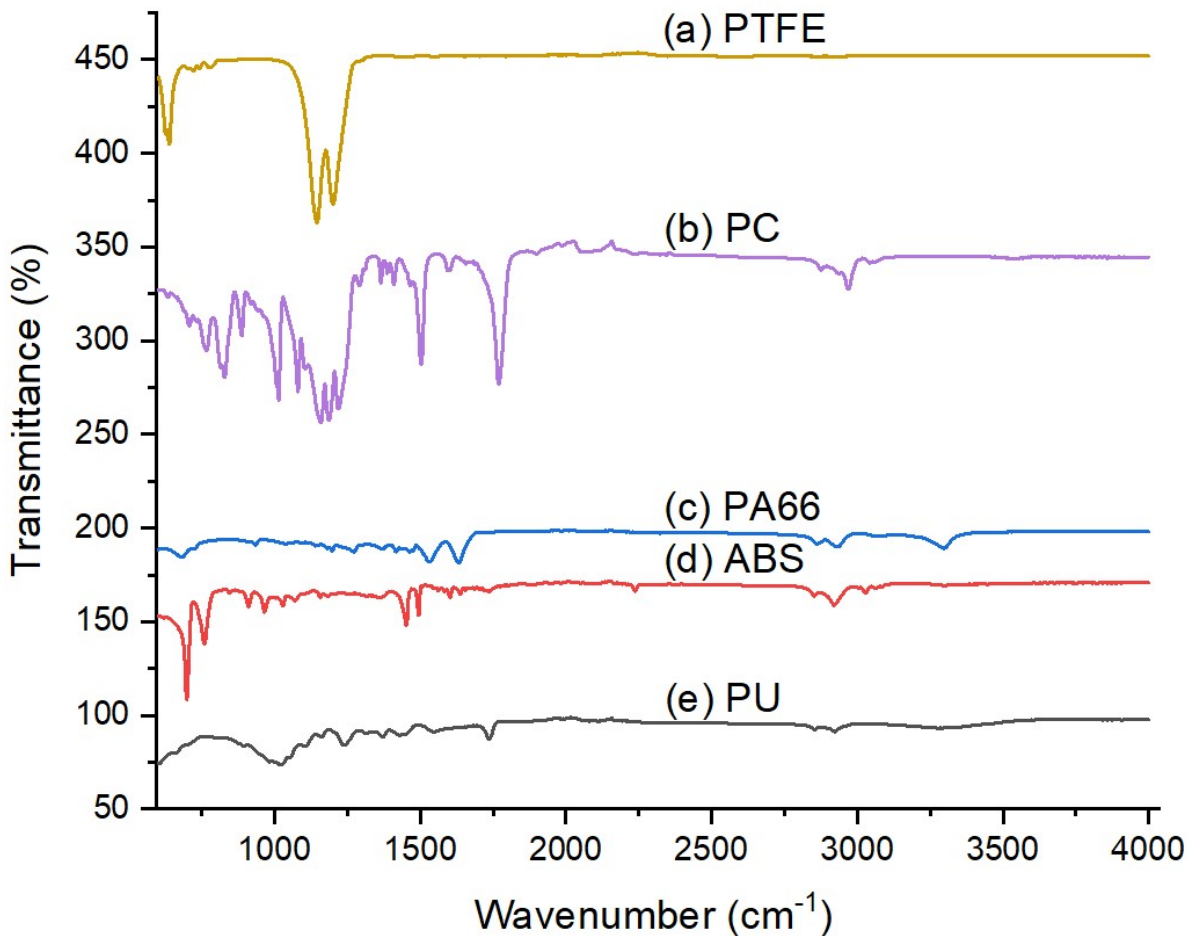


**Figure S7.** Original FTIR spectra of control samples: (a) polytetrafluoroethylene, (b) polycarbonate, (c) polyamide-66, (d) acrylonitrile butadiene styrene and (e) polyurethane.

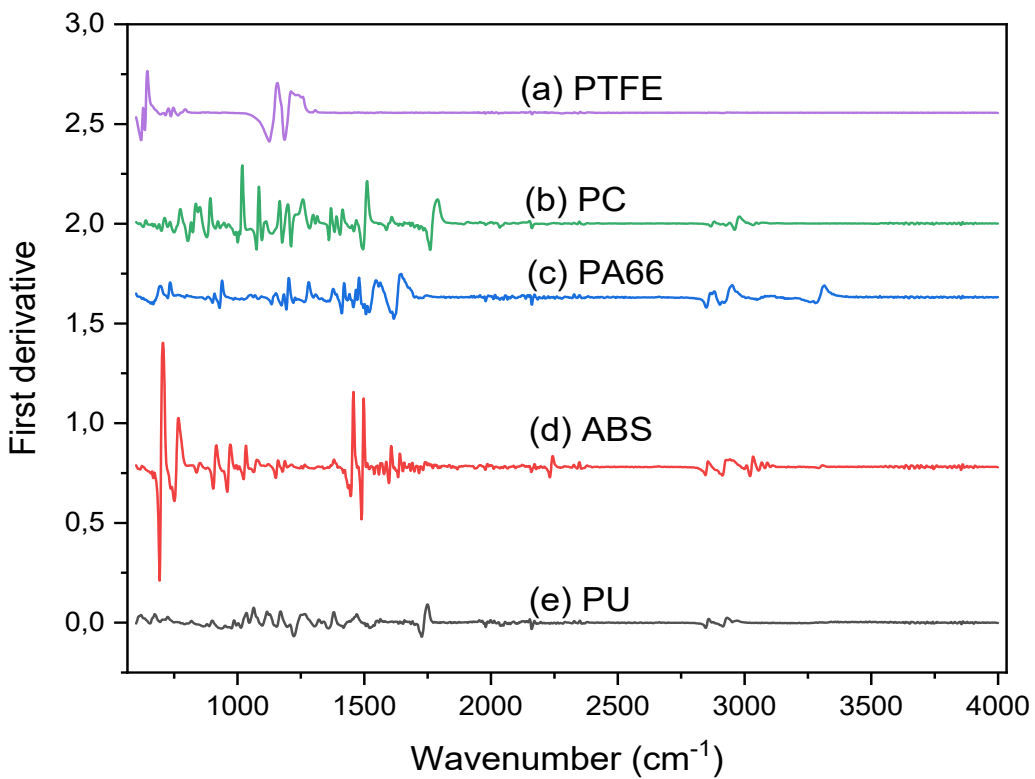


**Figure S8.** Preprocessed FTIR spectra of control samples: (a) polytetrafluoroethylene, (b) polycarbonate, (c) polyamide-66, (d) acrylonitrile butadiene styrene and (e) polyurethane

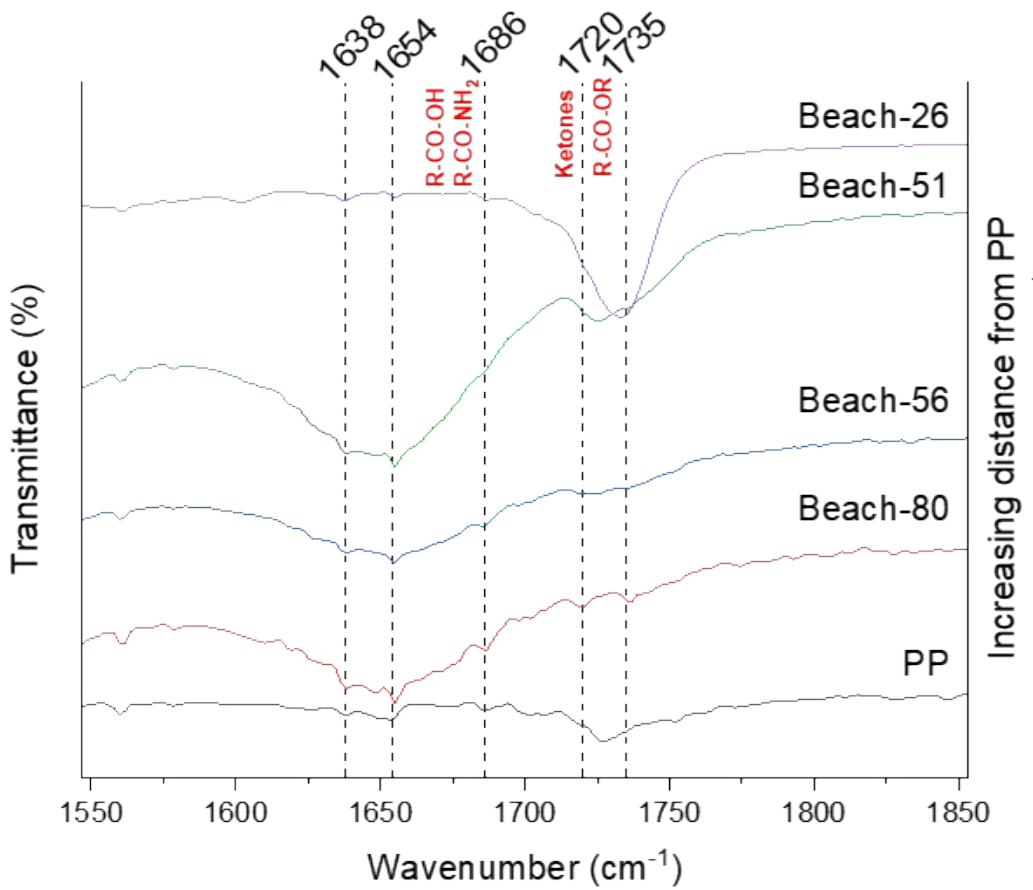


**Figure S9.** Zoom in on the carbonyl region ( $1650\text{-}1800\text{ cm}^{-1}$ ) of unprocessed FTIR spectra showing the various chemical groups that can be present on weathered plastics compared to a PP standard. Distance from PP in the right axis refers to the distance between the sample and the PP standard in the coordinates of Figure 4A. The peaks  $1640$  and  $1670\text{ cm}^{-1}$  suggest the presence of adsorbed water<sup>3</sup>.

Note: A few characteristic peaks were encountered in the carbonyl region like the presence of the amide/carboxyl group at  $1686\text{ cm}^{-1}$  or the vinyl, ketone and ester functions at  $1530\text{-}1680\text{ cm}^{-1}$ ,  $1720\text{ cm}^{-1}$  and  $1735\text{ cm}^{-1}$ , respectively. In other studies, perester ( $1770\text{ cm}^{-1}$ ) and  $\gamma$ -lactone ( $1795\text{ cm}^{-1}$ ) were also detected in this region<sup>4</sup>. Although a polyolefin is initially considered as an inert material (i.e., a weakly reactive hydrocarbon skeleton), it is very susceptible to photo-oxidation and charge transfer complexes<sup>5</sup>. Therefore, many chemical changes can occur inside the polymer chains during their life cycle. Besides, it is worthy to note that the type of photo-oxidation by-products can be modified by varying the exposure parameters. Indeed, an increase in the ratio light intensity/temperature favors the formation of esters at  $1735\text{ cm}^{-1}$  whereas the opposite trend leads to carboxylic acids (dimer form) peaking at  $1713\text{ cm}^{-1}$ <sup>6</sup>. Meanwhile, the amide bond detected at  $1686\text{ cm}^{-1}$  suggests a previous microbial attachment, therefore supporting the formation of biofilm on the plastic's surface<sup>3</sup>.

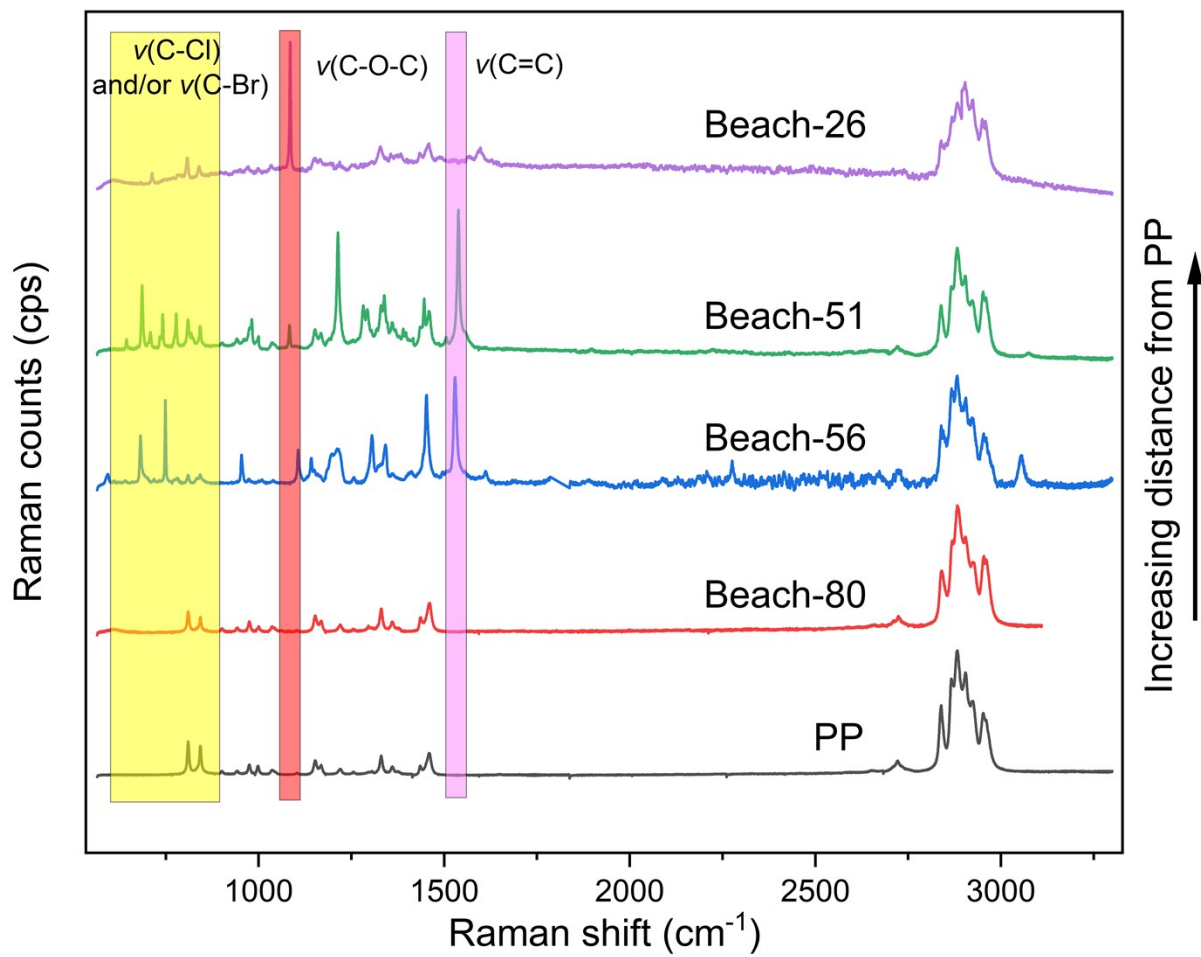


**Figure S10.** Raman spectra of the selected unidentified samples compared to the PP standard. Distance from PP in the right axis refers to the distance between the sample and the PP standard in the coordinates of Figure 4A.

**Table S5.** Raman shifts in  $\text{cm}^{-1}$  of selected samples ( $\rho$  : rocking,  $\nu$  : stretching,  $\delta$  : bending,  $\omega$  : wagging and  $\tau$  : twisting modes, \* indicates a non-assigned).

PP	Beach-80	Beach-56	Beach-51
2954 (vCH <sub>3</sub> asym.) 2902 (vCH) 2881 (vCH <sub>3</sub> sym.) 2868 (vCH <sub>2</sub> sym.) 2840 (vCH <sub>2</sub> sym.) 1458 ( $\delta\text{CH}_3$ asym., $\delta\text{CH}_2$ ) 1434 ( $\delta\text{CH}_3$ asym.) 1361 ( $\delta\text{CH}_3$ sym., $\delta\text{CH}$ ) 1328 ( $\delta\text{CH}$ , $\tau\text{CH}_2$ ) 1256 ( $\delta\text{CH}$ , $\tau\text{CH}_2$ , $\rho\text{CH}_3$ ) 1220 ( $\tau\text{CH}_2$ , $\delta\text{CH}$ , vCC <sub>b</sub> ) 1169 (vCC <sub>b</sub> , $\rho\text{CH}_3$ , $\delta\text{CH}$ ) 1153 (vCC <sub>b</sub> , vC-CH <sub>3</sub> , $\delta\text{CH}$ , $\rho\text{CH}_3$ ) 1041 (vC-CH <sub>3</sub> , vCC <sub>b</sub> , $\delta\text{CH}$ ) 996 ( $\rho\text{CH}_3$ , $\delta\text{CH}$ , $\omega\text{CH}_2$ ) 973 ( $\rho\text{CH}_3$ , vCC <sub>b</sub> ) 842 ( $\rho\text{CH}_2$ , vCC <sub>b</sub> , vC- CH <sub>3</sub> , $\rho\text{CH}_3$ ) 812 ( $\rho\text{CH}_2$ , vCC <sub>b</sub> , vC- CH <sub>3</sub> )	2954 (vCH <sub>3</sub> asym.) 2923 (vCH <sub>2</sub> asym.) 2904 (vCH) 2884 (vCH <sub>3</sub> sym.) 2869 (vCH <sub>2</sub> sym.) 2839 (vCH <sub>2</sub> sym.) 1459 ( $\delta\text{CH}_3$ asym., $\delta\text{CH}_2$ ) 1435 ( $\delta\text{CH}_3$ asym.) 1358 ( $\delta\text{CH}_3$ sym., $\delta\text{CH}$ ) 1329 ( $\delta\text{CH}$ , $\tau\text{CH}_2$ ) 1294 ( $\omega\text{CH}_2$ , $\delta\text{CH}$ , $\tau\text{CH}_2$ ) 1257 ( $\delta\text{CH}$ , $\tau\text{CH}_2$ , $\rho\text{CH}_3$ ) 1219 ( $\tau\text{CH}_2$ , $\delta\text{CH}$ , vCC <sub>b</sub> ) 1167 (vCC <sub>b</sub> , $\rho\text{CH}_3$ , $\delta\text{CH}$ ) 1153 (vCC <sub>b</sub> , vC-CH <sub>3</sub> , $\delta\text{CH}$ , $\rho\text{CH}_3$ ) 1035 (vC-CH <sub>3</sub> , vCC <sub>b</sub> , $\delta\text{CH}$ ) 1001 ( $\rho\text{CH}_3$ , $\delta\text{CH}$ , $\omega\text{CH}_2$ ) 975 ( $\rho\text{CH}_3$ , vCC <sub>b</sub> ) 943 ( $\rho\text{CH}_3$ , vCC <sub>b</sub> ) 903 ( $\rho\text{CH}_3$ , $\rho\text{CH}_2$ , $\delta\text{CH}$ ) 844 ( $\rho\text{CH}_2$ , vCC <sub>b</sub> , vC- CH <sub>3</sub> , $\rho\text{CH}_3$ ) 810 ( $\rho\text{CH}_2$ , vCC <sub>b</sub> , vC- CH <sub>3</sub> ) <u>605</u> (vC-Cl or vC-Br)	<u>3053</u> 2954 (vCH <sub>3</sub> asym.) 2923 (vCH <sub>2</sub> asym.) 2903 (vCH) 2882 (vCH <sub>3</sub> sym.) 2866 (vCH <sub>2</sub> sym.) 2844 (vCH <sub>2</sub> sym.) <u>1785</u> (vC=O) <u>1531</u> vs (vC=C) 1453 ( $\delta\text{CH}_3$ asym., $\delta\text{CH}_2$ ) 1358 ( $\delta\text{CH}_3$ sym., $\delta\text{CH}$ ) <u>1340</u> * 1307 ( $\omega\text{CH}_2$ , $\tau\text{CH}_2$ ) 1256 ( $\delta\text{CH}$ , $\tau\text{CH}_2$ , $\rho\text{CH}_3$ ) 1213 ( $\tau\text{CH}_2$ , $\delta\text{CH}$ , vCC <sub>b</sub> ) 1195* ( $\tau\text{CH}_2$ , $\delta\text{CH}$ , vCC <sub>b</sub> ) 1143 (vCC <sub>b</sub> , $\delta\text{CH}$ ) 1105 (vCC <sub>b</sub> , $\rho\text{CH}_3$ , $\omega\text{CH}_2$ , $\tau\text{CH}$ , $\delta\text{CH}$ ) <u>953</u> * 842 ( $\rho\text{CH}_2$ , vCC <sub>b</sub> , vC-CH <sub>3</sub> , $\rho\text{CH}_3$ ) 833 (vCC <sub>b</sub> , $\rho\text{CH}_3$ ) 810 ( $\rho\text{CH}_2$ , vCC <sub>b</sub> , vC-CH <sub>3</sub> ) <u>781</u> (vC-Cl) <u>747</u> (vC-Cl) <u>681</u> (vC-Cl or vC-Br) <u>591</u> (vC-Cl or vC-Br)	2951 (vCH <sub>3</sub> asym.) 2924 (vCH <sub>2</sub> asym.) 2903 (vCH) 2884 (vCH <sub>3</sub> sym.) 2867 (vCH <sub>2</sub> sym.) 2840 (vCH <sub>2</sub> sym.) <u>1541</u> vs (vC=C) 1461 ( $\delta\text{CH}_3$ asym., $\delta\text{CH}_2$ ) <u>1445</u> * 1437 ( $\delta\text{CH}_3$ asym.) 1398* 1390* 1360 ( $\delta\text{CH}_3$ sym., $\delta\text{CH}$ ) <u>1340</u> * 1332 ( $\delta\text{CH}$ , $\tau\text{CH}_2$ ) 1292 ( $\omega\text{CH}_2$ , $\delta\text{CH}$ , $\tau\text{CH}_2$ ) <u>1284</u> * 1216 ( $\tau\text{CH}_2$ , $\delta\text{CH}$ , vCC <sub>b</sub> ) 1170 (vCC <sub>b</sub> , $\rho\text{CH}_3$ , $\delta\text{CH}$ ) 1150 (vCC <sub>b</sub> , vC-CH <sub>3</sub> , $\delta\text{CH}$ , $\rho\text{CH}_3$ ) <u>1083</u> * 1034 (vC-CH <sub>3</sub> , vCC <sub>b</sub> , $\delta\text{CH}$ ) 1000 ( $\rho\text{CH}_3$ , $\delta\text{CH}$ , $\omega\text{CH}_2$ ) <u>981</u> * 941 ( $\rho\text{CH}_2$ , vCC <sub>b</sub> ) 843 ( $\rho\text{CH}_2$ , vCC <sub>b</sub> , vC- CH <sub>3</sub> , $\rho\text{CH}_3$ ) <u>819</u> * 810 ( $\rho\text{CH}_2$ , vCC <sub>b</sub> , vC- CH <sub>3</sub> ) <u>778</u> (vC-Cl) <u>741</u> (vC-Cl) <u>734</u> (vC-Cl) <u>708</u> (vC-Cl) 685 (vC-Cl or vC-Br) 643 (vC-Cl or vC-Br)

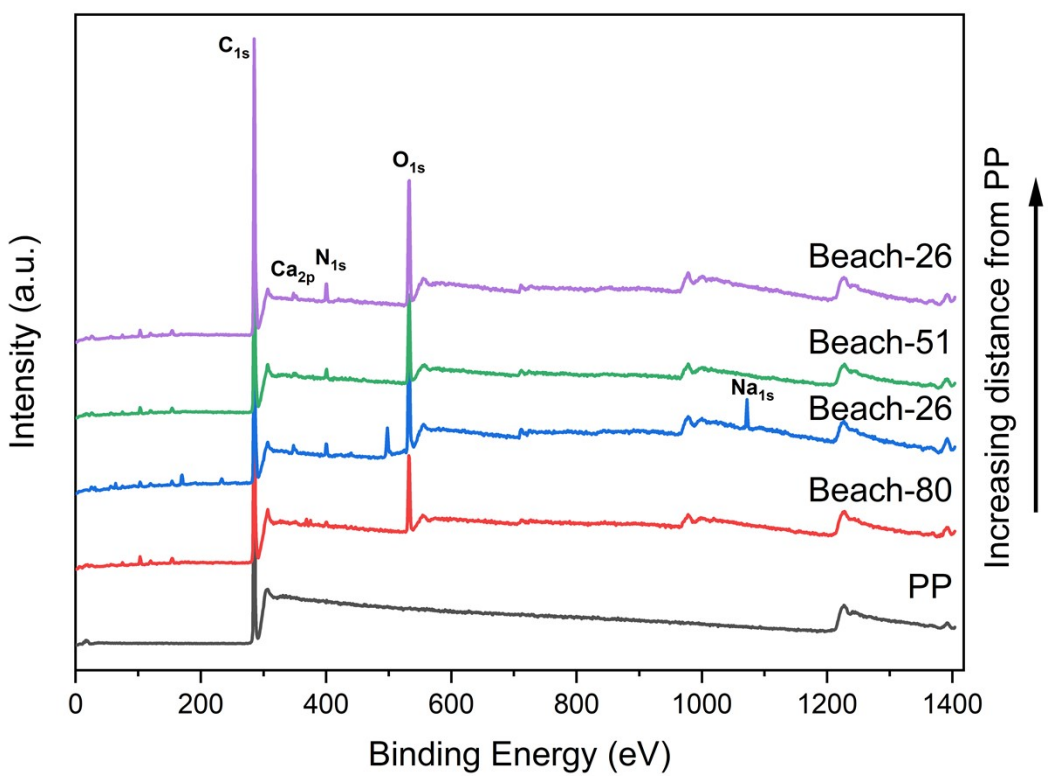


**Figure S11.** XPS survey spectra of the selected unidentified samples and PP. Distance from PP in the right axis refers to the distance between the sample and the PP standard in the coordinates of Figure 4A.

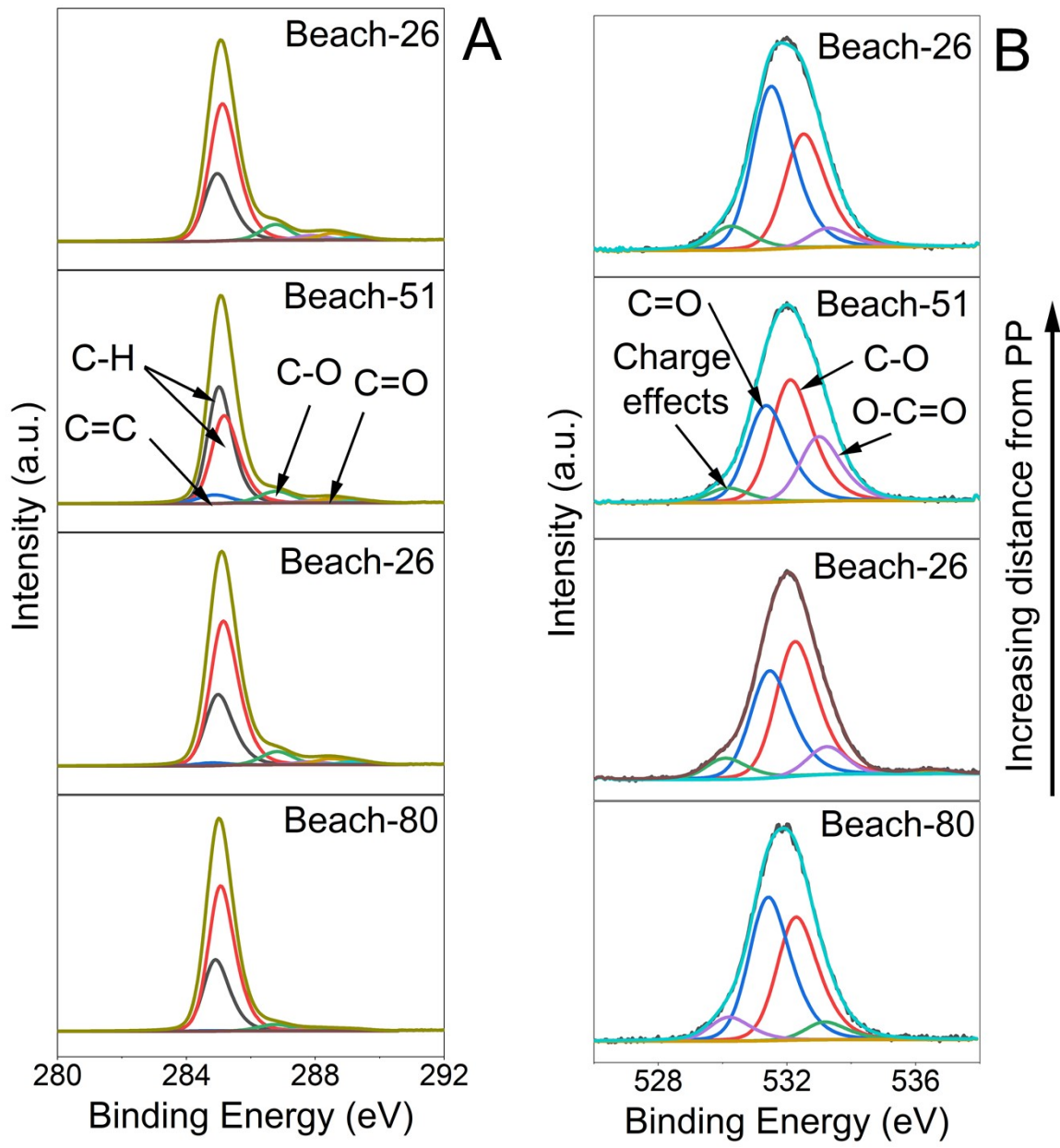
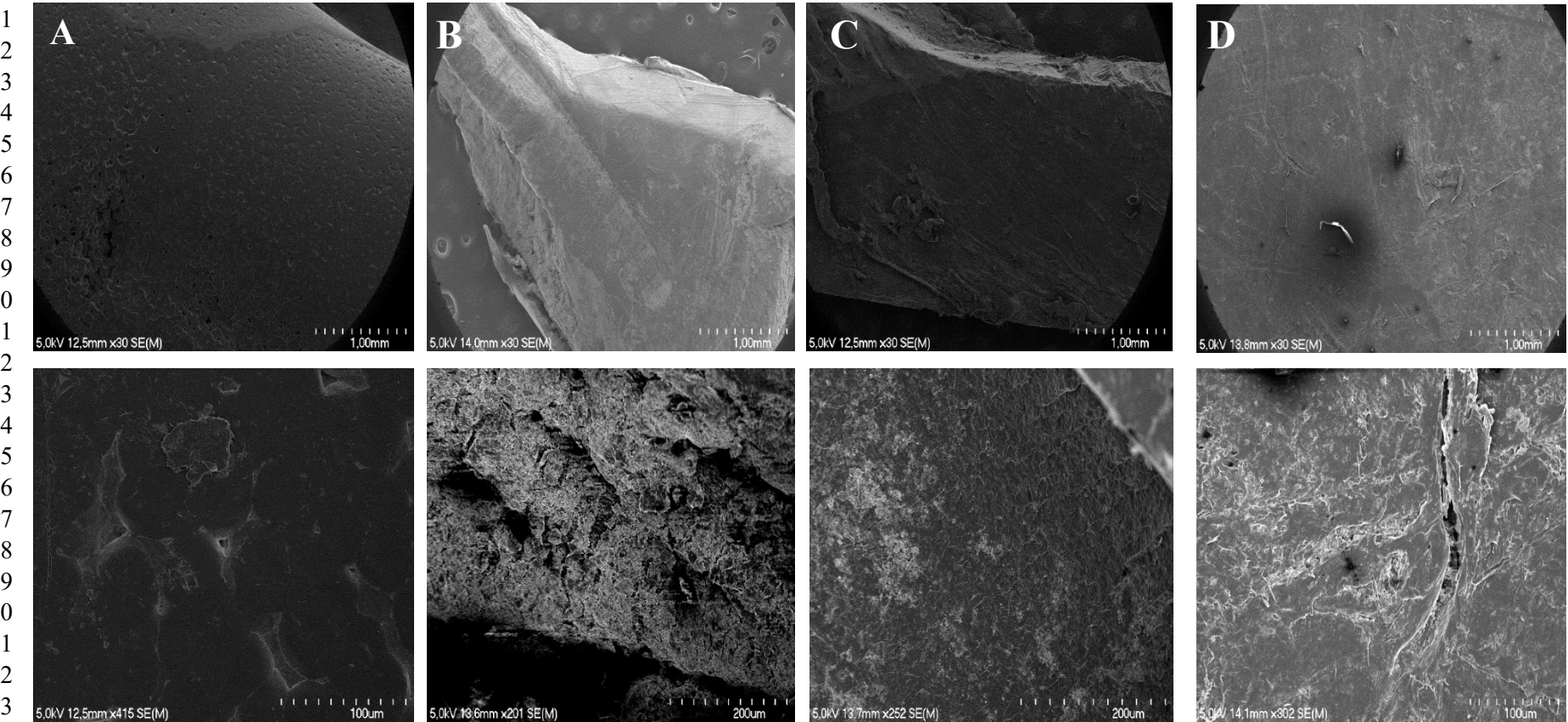


**Figure S12.** High-resolution XPS spectra of beach samples **A:** C<sub>1s</sub> For these spectra, aliphatic hydrocarbon -CH<sub>n</sub> (Binding energy=285.0 eV), alkenes (B.E.=284.7 eV), ether and/or alcohol (B.E.=286.7 eV), carbonyl (B.E.=287.8 eV) and carboxylic acid (B.E.=289.2 eV) explain most of the shape of the signals obtained. **B:** O<sub>1s</sub>. For these spectra, three peaks are sufficient to explain the shape of the signals obtained: C-O-C or C-OH (B.E.=532.8 eV), C=O (B.E.=531.8 eV) and O=C-O (B.E.=533.7 eV). An additional peak originates from the inhomogeneous charge effects due to the insulating nature of the materials tested (B.E.=530.5 eV). Distance from PP in the right axis refers to the distance between the sample and the PP standard in the coordinates of Figure 4A. In general,



25 **Figure S13.** SEM images of A: PP standard; B: Beach-56; C: Beach-51 and D: Beach-26. Top images were taken with a magnification set at 30×.  
26 Bottom images were taken with a magnification ranging from 200× to 415×.

27 **Notes on SEM analysis**

28

29 The surface of the PP standard is relatively flat and smooth with few mechanical pits, which  
30 could be a direct consequence of the sample pressing with ZnSe crystal in ATR-FTIR  
31 technique. Compared to standard PP, the selected beach samples showed much more prominent  
32 structural irregularities, including grooves, solution pits, i.e., oxidative texture caused by  
33 dissolution of structurally weaker materials, such as pigments, additives and antioxidants<sup>7</sup>,  
34 horizontal notching, flakes, as well as linear and vermiculite (worm-like) fractures. These  
35 surface textures are the result of two different processes that occurred in the environment:  
36 mechanical and oxidative weathering<sup>7</sup>, with each category having its own characteristic  
37 textures.

38

39 **References**

40

- 41 1. D. Atek and N. Belhaneche-Bensemra, *Eur. Polym. J.*, 2005, **41**, 707-714.  
42 2. R. Stringer, I. Labunská, D. Santillo, P. Johnston, J. Siddorn and A. Stephenson,  
43 *Environ. Sci. Poll. Res.*, 2000, **7**, 27-36.  
44 3. M. Dong, Q. Zhang, X. Xing, W. Chen, Z. She and Z. Luo, *Sci. Total Environ.*, 2020,  
45 **739**, 139990.  
46 4. A. Tidjani, *J. Appl. Polym. Sci.*, 1997, **64**, 2497-2503.  
47 5. P. Gijsman, G. Meijers and G. Vitarelli, *Polym. Degrad. Stab.*, 1999, **65**, 433-441.  
48 6. J.-L. Philippart, C. Sinturel, R. Arnaud and J.-L. Gardette, *Polym. Degrad. Stab.*, 1999,  
49 **64**, 213-225.  
50 7. M. Zbyszewski, P. L. Corcoran and A. Hockin, *J. Great Lakes Res.*, 2014, **40**, 288-  
51 299.

52